Bull. Mater. Sci., Vol. 32, No. 6, December 2009, pp. 643–652. © Indian Academy of Sciences.

A comprehensive study on the effect of Ru addition to Pt electrodes for direct ethanol fuel cell

J DATTA*, S SINGH, S DAS† and N R BANDYOPADHYAY†

Department of Chemistry, †School of Materials Science and Engineering,
Bengal Engineering and Science University, Shibpur, Howrah 711 103, India

MS received 24 October 2008; revised 3 January 2009

Abstract. **The electro-oxidation of ethanol was studied over nanosized Pt and different compositions of PtRu catalysts synthesized by the borohydride reduction method. Physicochemical characterizations of the catalyst material were made by X-ray diffraction (XRD), scanning electron microscopy (SEM) coupled with EDX analysis and transmission electron microscopy (TEM). XRD patterns showed that Ru induces a contraction of the Pt lattice. EDX provided the composition of binary catalysts while TEM images indicated uniform distribution of discrete nanoparticle of the catalysts with narrow range. The electro-catalytic activities of the materials towards ethanol oxidation were investigated through electrochemical techniques, viz. cyclic voltammetry (CV), potentiodynamic polarization, chronoamperometry (CA) and electrochemical impedance spectroscopy (EIS) at room temperature. The onset potential of ethanol electro-oxidation is lowered on bimetallic PtRu catalysts compared to that on Pt alone. Of the investigated catalyst compositions the one with the highest electro-catalytic activity was found to be $Pt_{82}Ru_{18}$. This enhancement towards ethanol oxidation is explained on the basis of a structural effect and modified bi-functional mechanism.**

Keywords. **Ethanol electrooxidation; PtRu alloy catalysts; electro catalytic activity; charge transfer resistance.**

1. Introduction

Despite significant efforts to improve the power performance of pure hydrogen or reformate gas proton exchange membrane fuel cells (PEMFCs) using pure or reformed hydrogen, there are still many technological hurdles to overcome before its commercialization as stationary and vehicular power sources (O'Hayre *et al* 2006). This is due largely to difficulties in hydrogen supply infrastructure or fuel reforming technology associated with cleaning up of impurities such as CO and sulphur compounds.

In recent times the PEM-based direct alcohol fuel cell (DAFC) is receiving increased attention due to its much simpler peripheral units than those of the H_2–O_2 PEMFC systems, such as easy fuel delivery and storage, no need for reforming, humidification and stack cooling, and favourable power capability (Lamy *et al* 2001). Liquid fuels, such as methanol and ethanol, featuring higher volumetric and gravimetric energy densities and better energy efficiency, can be easily handled, stored and transported in comparison with gaseous fuels. During the past decade, direct methanol fuel cell (DMFC) has been widely investigated (Arico *et al* 1996; Wasmus and Kuver 1999; Hogarth and Ralph 2002) and considered as a possible power source for electric vehicles and other portable applications for the future. However, environmental concerns limit the use of methanol as a friendly fuel since it is volatile and relatively toxic than other small alcohols. On the other hand, ethanol is non toxic and has more energy density compared to methanol (8·01 kWh/kg vs 6·09 kWh/kg) (Lamy *et al* 2002) and can be easily produced in great quantity by fermentation of sugar-containing raw materials. Therefore, ethanol is more attractive than methanol for direct alcohol fuel cells operating at lower temperature.

In direct ethanol fuel cell, ethanol is electro-oxidized at the anode and oxygen is reduced at the cathode according to reactions (1) and (2), respectively to result in the generation of electricity and heat.

Anode: $C_2H_5OH + 3\ H_2O \rightarrow 2CO_2 + 12H^+ + 12e$

$$E^0 = 0{\cdot}085\ \text{V}, \quad (1)$$

Cathode: $3O_2 + 12H^+ + 12e \rightarrow 6H_2O$

$$E^0 = 1{\cdot}23\ \text{V}, \quad (2)$$

Overall: $C_2H_5OH + 3O_2 \rightarrow 2CO_2 + 3H_2O$

$$E^0 = 1{\cdot}145\ \text{V}. \quad (3)$$

*Author for correspondence (jayati_datta@rediffmail.com)

The desired reaction in direct ethanol fuel cells is the complete oxidation of ethanol to CO_2 and water involving 12 electrons transfer per ethanol molecule. It is reported that ethanol electro-oxidation involves several pathways (Lamy *et al* 2001). The two major challenges viz. electro-oxidative removal of CO-like intermediates and the scission of the C–C bond still remain with the conversion process (Zhou *et al* 2004). Although attempts of increasing reaction temperature and adopting more active electrocatalysts can enhance the ethanol electrochemical reaction activity, the former is not, at least at present, the primary choice because the perfluorosulfonic-based polymer electrolyte membrane gets dehydrated at higher operation temperatures, resulting in the rise of reaction impedance and subsequent deterioration of fuel cell performance (Yang *et al* 2001).

It is well known that the structure, morphology and composition of the electrode material play a key role in the catalytic performance of alcohol electro-oxidation. When pure platinum electrode is used for ethanol electro-oxidation many problems such as auto-inhibition or poisoning phenomena arise resulting in high overpotentials (Rightmire *et al* 1964; Iwasita and Pastor 1994). In order to increase the electrocatalytic activity of platinum towards ethanol oxidation, a second oxophilic metal like Ru (Laborade *et al* 1994; Volkmar *et al* 1996; Fujiwara *et al* 1999; Chen *et al* 2001; Song *et al* 2005), Rh (De Souza *et al* 2002), Mo (Oliveria Neto *et al* 2002), Os (Pacheo *et al* http://www.Arofe.army.mil) or Sn (Delime *et al* 1999; Vigier *et al* 2004) is usually introduced as alloying metal, thus promoting the electrocatalytic activity of pure platinum. PtRu nano-clusters have been the most investigated of fuel cell catalysts (Watanabe and Motoo 1975a; Janssen and Moolhuysen 1977). The superior performance of this catalyst relative to pure Pt has been explained in terms of either of two models: the bi-functional mechanism and the ligand effect. In the bi-functional mechanism model, Ru atom was recognized as a provider of oxygen-containing species for the CO oxidative removal as shown below:

$$\text{Ru–OH} + \text{Pt–CO} \rightarrow \text{Ru} + \text{Pt} + \text{CO}_2 + \text{H}^+ + e^-.$$

The ligand effect, on the other hand, known as the electronic model, was based on the modification of Pt electronic structure by the presence of Ru making Pt atoms less poisoned by CO.

However, the ratio of the constituents in this binary catalyst has to be optimized because ethanol oxidation activity is known to be sensitive to the Pt : Ru content. This also includes varying the concentration of the surface oxide species. Detailed electrochemical and physical characterizations are therefore, required to understand the individual contribution of each of the constituents toward ethanol oxidation activity and in particular, the role of the surface oxide species. The mechanistic insights will form the basis for optimization of the catalyst composition for ethanol electro-oxidation.

In the present paper, we have studied the activity of chemically synthesized unsupported Pt and PtRu catalysts with different compositions towards the electro-oxidation of ethanol. The structure and morphology of the catalyst nanoparticles were determined by XRD, SEM and TEM. Electrochemical techniques like cyclic voltammetry, potentiodynamic polarization, chronoamperometry and electrochemical impedance spectroscopy (EIS) were used to investigate the catalytic activity towards electro-oxidation of ethanol.

2. Experimental

2.1 *Synthesis of unsupported catalysts*

Unsupported Pt and PtRu catalysts were synthesized in the powdered form by $NaBH_4$ reduction of appropriate molar concentrations of $H_2PtCl_6{\cdot}xH_2O$ and $RuCl_3{\cdot}6H_2O$ (Arora Matthey Ltd.). The mixtures were stirred for 1 h and subsequently appropriate quantities of 0·05 M $NaBH_4$ (Merck) solution were added, drop by drop, to the mixture with vigorous stirring for the complete reduction of Pt and/or Ru from their respective metal precursors. Subsequently the black colloidal mixtures were stirred for 30 min at room temperature. Finally the colloid was centrifuged, collected, washed with plenty of water and dried at 110°C. In case of binary catalysts, the stoichiometry corresponded to Pt : Ru molar ratios of 1 : 1, 5 : 1 and 10 : 1. Working electrodes were prepared using saw cut finish grade graphite plate (GLM, Graphite India Ltd) of thickness ~2 mm as electrode substrate. A catalyst ink was prepared by mixing appropriate amount of catalysts, Nafion ionomer (5 wt% solutions, Electrochem. Inc, USA) and 2-propanol (GR, Merck) and the mixture was sonicated. A fixed amount of this slurry was micropipetted out onto the graphite support (0·65 cm^2) maintaining a constant catalyst loading of 0·5 mg cm^{-2}.

2.2 *Physical characterization*

X-ray diffraction (XRD) patterns of the electrocatalysts were obtained in a SEIFERT 2000 diffractometer operating with CuK_α radiation (λ = 0·1540598 nm) generated at 35 kV and 30 mA. Scans were done at 1° min^{-1} for 2θ values between 20 and 90 degrees. Scherrer equation was used for the determination of particle size from XRD. For this purpose, the (111) peak of the Pt face centred cubic (*fcc*) structure was selected. The surface morphology of the electrocatalysts was investigated with a LEO S 430i scanning electron microscope at an accelerating potential of 20 kV. The chemical composition of the catalyst layers was determined by energy dispersive X-ray (EDX) using Link ISIS EDX detector (Oxford Instruments, UK) coupled with the scanning electron microscope. The morphology and the particle size distributions of PtRu catalysts were

analysed by TEM observation. At first, the catalysts were ultrasonically dispersed in ethanol solution to obtain uniform catalyst ink and mounted onto a copper grid covered with carbon film. A JEOL JEM 2100 microscope, operating at 200 kV, was used for TEM observation.

2.3 *Electrochemical measurements*

Electrochemical measurements were carried out using cyclic voltammetry (CV), potentiodynamic polarization studies, electrochemical impedance spectroscopy (EIS) and chronoamperometry with the help of a computer controlled potentiostat/galvanostat with PG STAT 12 and FRA modules (Eco Chemie BV, The Netherlands). A conventional H-type three-electrode cell consisting of catalyst coated graphite carbon with an area 0·65 cm^2 as the working electrode, Pt foil as counter electrode and mercury-mercurous sulphate (MSE) as reference electrode (0·68 V vs SHE) was used for electrochemical experiments. The electrolyte solution was de-aerated with pure nitrogen prior to each experiment. The CV experiments were performed in 0·5 M H_2SO_4 solution in the absence and presence of 1·0 M ethanol at a scan rate of 50 mV s^{-1}. Steady state potentiostatic data was recorded after polarization for 5 min. The chronoamperometric experiments were studied at –0·1 V for 1 h duration. EIS measurements were performed in the frequency range 30 kHz–30 mHz containing 40 data points. The amplitude of the a.c. signal was 5 mV.

3. Results and discussion

For the synthesis of binary catalysts, the borohydride method was adopted because of its procedural simplicity and proven effectiveness for synthesizing nanoparticles. The simultaneous reduction of metal salts has several intrinsic advantages, viz. assurance of molecular level mixing between the constituent metals and a predetermined stoichiometry based on the atomic composition in the precursor. For the present study the stoichiometry of the reduction reactions can be summarized as follows:

$$2PtCl_6^{2-} + BH_4^- + 4H_2O \rightarrow 2Pt + B(OH)_4^- + 8H^+ + 12Cl^-,$$

$$8Ru^{3+} + 3BH_4^- + 12H_2O \rightarrow 8Ru + 3B(OH)_4^- + 24H^+.$$

The relative atomic Pt : Ru ratios of the chemically synthesized catalysts were determined by EDX analysis (table 1).

3.1 *SEM, EDX and TEM characterizations*

In order to investigate the morphology of the chemically synthesized unsupported Pt and PtRu catalysts, the samples were examined through scanning electron microscopy. A direct evaluation of the particle size is not possible for these Pt deposits which appear to be agglomerated for the SEM images. Figure 1 shows a typical SEM image of the $Pt_{91}Ru_9$ electrode surface. It shows catalyst particle sizes lie within a few nanometers and are in good agreement with the average particle size obtained from XRD measurement described in the following section. Figure 2 is a typical EDX spectrum of unsupported $Pt_{91}Ru_9$ catalyst. The EDX data show that the Pt : Ru atomic ratios of the obtained electrocatalysts were close to the nominal atomic ratios used during synthesis (table 1). HRTEM image of $Pt_{82}Ru_{18}$ catalyst particles, shown in figure 3, allowed direct measurement of the particle size distribution. In general, the PtRu alloy nanoparticles are spherical in shape and are 3–5 nm in size range. A representative selected area electron diffraction (SAED) pattern of the synthesized catalysts reveals the crystalline planes of the nanoparticles as shown in figure 4. Further the concentric rings are indexed for the *fcc* structure of the Pt crystal lattice.

3.2 *X-ray diffraction (XRD)*

XRD provides the information on the bulk structure of the catalyst. Figure 5 shows the XRD patterns of unsupported Pt and PtRu catalysts. The XRD patterns of Pt can be indexed to the diffraction peaks of (111), (200), (220), (311) and (222) planes corresponding to a face centred cubic (*fcc*) structure (Liu *et al* 2005; Li *et al* 2007). All the PtRu catalysts prepared with different molar ratios of Pt : Ru displayed the diffraction peaks similar to those of Pt metal except that the 2θ values were shifted to slightly higher values. For instance, the 2θ of the (111) peaks of Pt and different molar ratios of PtRu such as (91 : 9), (82 : 18) and (50 : 50) are found at 39·829, 40·005, 40·030 and 40·084, respectively (figure 6). Such evidence

Table 1. Ratio of Pt and Ru precursor salts used in synthesis and that obtained on the PtRu catalysts as determined by EDX analysis.

H_2PtCl_6 (M)	$RuCl_3$ (M)	% Pt (from EDX)	% Ru (from EDX)	Pt/Ru (solution)	Pt/Ru (catalyst)
$2·0 \times 10^{-2}$	$2·0 \times 10^{-3}$	90·9	9·1	10	9·9
$2·0 \times 10^{-2}$	$4·0 \times 10^{-3}$	81·6	18·4	5	4·4
$2·0 \times 10^{-2}$	$2·0 \times 10^{-2}$	50·3	49·7	1	1·01

accounts for the formation of PtRu alloy in the catalysts. However, the peaks associated with a typical hexagonal closed packed (*hcp*) structure of pure ruthenium or ruthenium oxide phase did not appear in the XRD pattern of PtRu catalysts (Colmati *et al* 2002; Spinace *et al* 2004). Despite the absence of such peaks, some amount of metallic Ru and its oxides in the amorphous state may always exist in the PtRu catalyst. The lattice parameter (a) values of the Pt and PtRu alloy based nanocatalysts with different molar ratios of Pt : Ru was calculated from broadening of the (111) diffraction peak and listed in table 2. Consistent with the literature data, the $Pt_{50}Ru_{50}$ catalyst has a much smaller lattice parameter (a = 3·8916 nm) (Colmati *et al* 2007) and this may indicate that the addition of the secondary metal Ru has a considerable influence on the crystal structure of Pt catalyst (Li *et al* 2007). This can be explained by its different atomic size as against that of Pt element (R_{Pt} = 1·39 Å and R_{Ru} = 1·34 Å). However, the lattice parameter of 3·9155 Å for the prepared Pt catalyst is in good agreement with the literature value of 3·923 Å for pure Pt (JCPDS 04-0802). The average crystallite size and lattice parameters for the PtRu alloys prepared with different molar ratios of Pt : Ru was calculated from broadening of the (111) diffraction peak using Scherrer equation and is listed in table 2. The composition of the PtRu catalysts was further determined with the help of Vegard's law, from the shift of Pt diffraction peaks, or the variation of the lattice parameter from the XRD patterns. From literature data (Chu and Gilman 1996), a linear relationship of the lattice parameter and the alloyed Ru atomic fraction (<0·7) has been proposed:

$$a(\text{Pt–M}) = a(\text{Pt}) - kx(\text{Ru}), \quad (1)$$

where a (Pt) and a (Pt–M) represent the lattice parameter of Pt and the Pt–Ru alloyed catalyst, respectively. The value of constant k = 0·124 Å was taken from literature (Li *et al* 2007). According to this equation, the atomic content of alloyed Ru [x(Ru)] in our PtRu samples like $Pt_{91}Ru_9$, $Pt_{82}Ru_{18}$ and $Pt_{50}Ru_{50}$ are 0·1323, 0·1512 and 0·1918, respectively which are summarized in table 2. Figure 7 is a plot of the evaluated lattice parameters as a function of at. % Pt (as obtained from EDX) in PtRu catalysts.

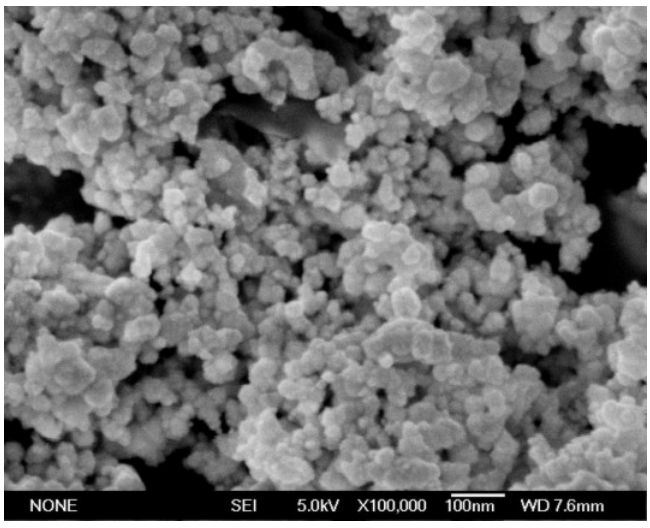

Figure 1. SEM images of chemically synthesized unsupported $Pt_{91}Ru_9$.

3.3 *Cyclic voltammetric study in base electrolyte*

Figures 8(a)–(c) show a comparison of the cyclic voltammograms of Pt and PtRu catalysts of different stoichiometries in 0·5 M H_2SO_4. The upper potential limit was restricted to 0·2 V vs MSE because beyond this potential Ru dissolutes from the electrode surface during multiple scanning. With increasing Ru content in the binary catalysts the current-potential peaks in the hydrogen-adsorption region become broader and less defined than on pure Pt. Following the hydrogen region, the double layer region for the Pt electrode is narrow and featureless. The current slowly rises at 0·10 V potential indicating the formation of surface oxides. In contrast, the current response in the double layer region of the PtRu electrodes becomes progressively broader with increasing Ru. This can be accounted for by the reversible formation and reduction of surface Ru oxides in this potential region, the amount of which increases with the Ru content of the catalysts. The position of the oxide reduction peak in the negative going sweep shifts to lower potentials for electrodes with higher Ru content. This agrees well with the results of McNicol and Short (1978), Mahmood *et al* (1981) and Frelink *et al*'s (1995) findings although they had adopted a different synthetic method for PtRu alloys and PtRu codeposited electrodes, respectively. The major change in the voltammetric response due to the incorporation of Ru on the Pt surface is the increasing double layer currents over that of Pt indicating the adsorption of oxygen-like species at progressively more negative potentials as compared to Pt itself.

3.4 *Cyclic voltammograms of ethanol electro oxidation*

Figure 9 compares the ethanol oxidation behaviour over Pt and PtRu catalysts. A higher efficiency for ethanol oxidation at more negative potentials i.e. at lower overpotentials, is obtained with the PtRu catalysts. In this respect, $Pt_{82}Ru_{18}$ displays the highest activity amongst all catalyst formulations employed in this study. The enhancement of activity of these binary catalysts towards ethanol electro-oxidation can be related to their superior CO tolerance. The effect of adding Ru on ethanol oxidation is explained by the well known bifunctional mechanism (Watanabe and Motoo 1975b; Iwasita 2002):

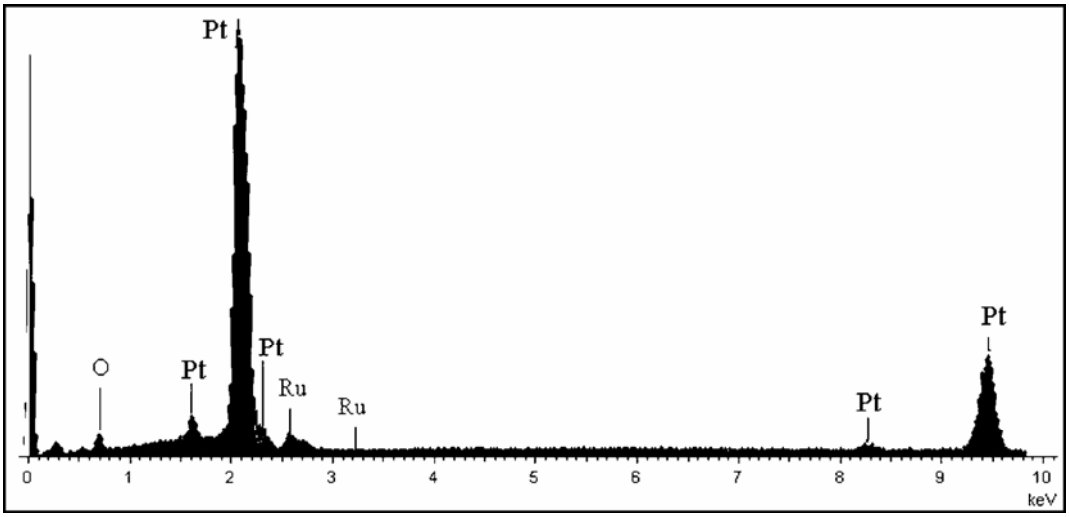

Figure 2. EDX spectrum of the unsupported $Pt_{91}Ru_9$ catalyst.

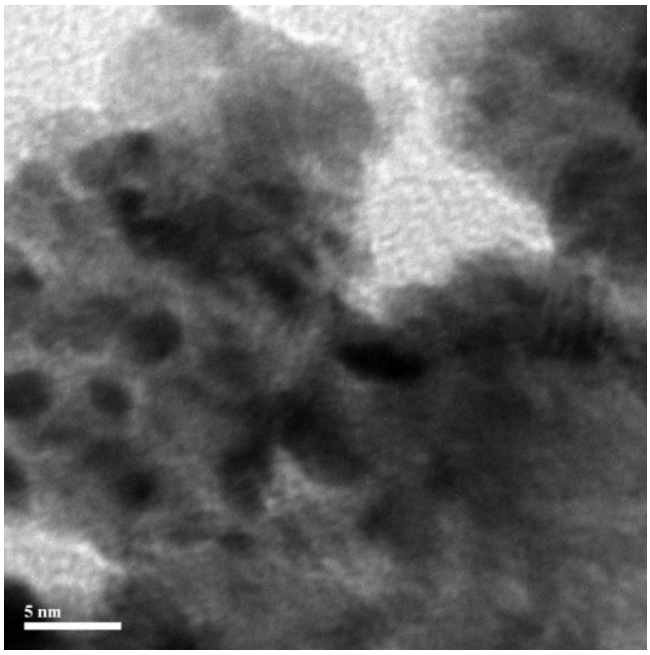

Figure 3. HRTEM image of the unsupported $Pt_{82}Ru_{18}$.

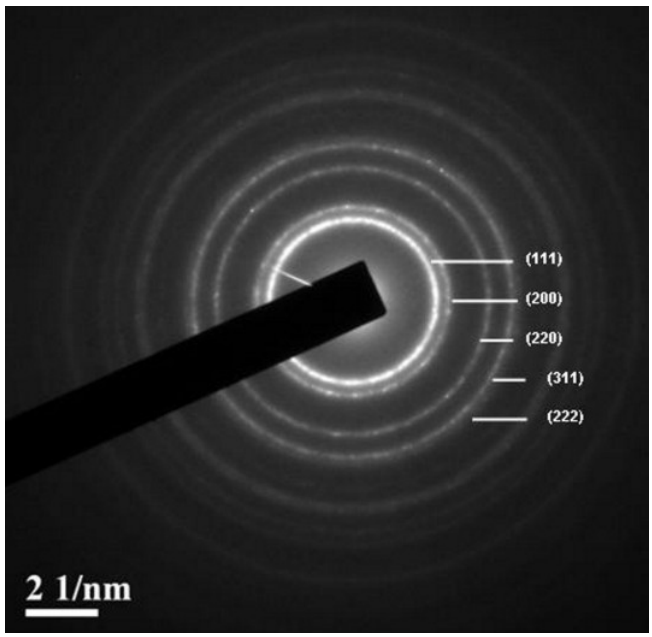

Figure 4. Selected area electron diffraction (SAED) pattern of $Pt_{82}Ru_{18}$ catalyst. The rings are indexed for an *fcc* crystal structure.

$$Pt + CO \rightarrow Pt\text{–}CO_{ad},$$

$$Ru + H_2O \rightarrow Ru\text{–}OH_{ad} + H^+ + e^-,$$

$$Pt\text{–}CO_{ad} + Ru\text{–}OH_{ad} \rightarrow CO_2 + H^+ + e^-.$$

Ethanol is adsorbed on the Pt surface and is oxidized to CO. Although Ru itself has been found to be inactive for ethanol oxidation, Ru oxidatively decomposes water and OH is adsorbed on the Ru surface. Thus, Ru supplies oxygen species for CO oxidation and promotes ethanol oxidation. The OH adsorption on the Ru surface commences at –0·35 V, which shifts the onset potential of ethanol oxidation in the negative direction. However, this lowering of the onset potential is progressively reduced on moving towards higher Ru content, until for the $Pt_{50}Ru_{50}$ catalyst composition the current response almost merges with that of Pt in the –0·25 to 0·1 V potential window. The lowering of the oxidation current with increasing Ru content is probably a manifestation of the drastic reduction in the number of ethanol adsorption sites on the $Pt_{50}Ru_{50}$ catalyst surface as compared to Pt alone.

The onset potential for ethanol oxidation is an important parameter for judging the activity of Pt-based electrocatalysts operating through a bifunctional mechanism. From figure 9(a) it is quite clear that in the hydride

Table 2. Average crystallite size and lattice parameter of the Pt and PtRu catalysts compositions obtained from XRD measurements.

Catalysts	2θ (degrees)	Full width at half maxima (Å)	Average crystallite size (nm)[a]	Lattice parameter (Å)[b]	X_{Ru}[c]
Pt	39·829	2·8431	2·97	3·9155	–
$Pt_{91}Ru_9$	40·005	1·4116	5·99	3·8990	0·1323
$Pt_{83}Ru_{17}$	40·030	1·6738	5·05	3·8966	0·1512
$Pt_{50}Ru_{50}$	40·084	3·7301	2·3	3·8916	0·1918

[a]Calculated from Pt (111) peak position according to Scherrer formula; [b]calculated from Pt (111) peak according to Bragg formula; [c]mole fraction of Ru in the alloyed state (X_{Ru}) calculated from Vegard's law

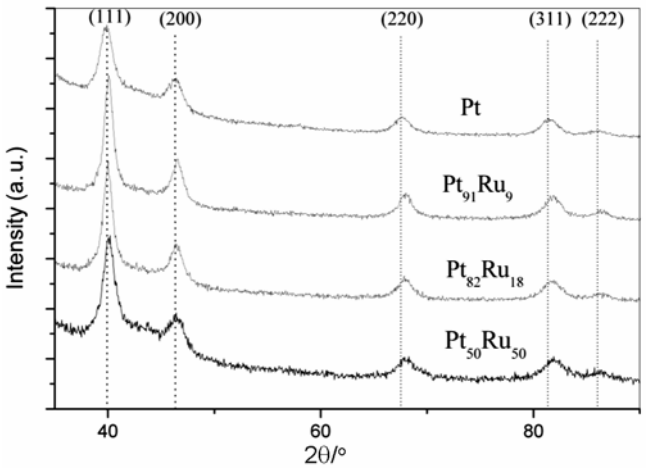

Figure 5. X-ray diffraction patterns of platinum and platinum-ruthenium catalysts.

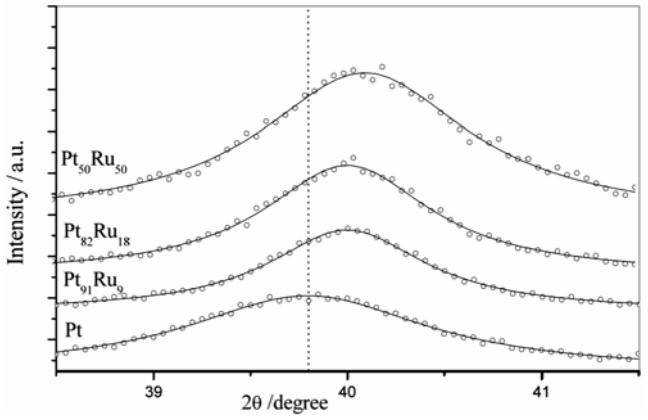

Figure 6. (111) diffractions of Pt and PtRu electrocatalysts.

region ethanol adsorption current of $Pt_{82}Ru_{18}$ is higher in comparison to other catalysts. The oxidation current of $Pt_{82}Ru_{18}$ commences sharply at a negative potential of –0·4 V whereas, the other catalysts suffer a decreasing current trend at the same potential and the oxide currents start at a much higher potential than that for $Pt_{82}Ru_{18}$.

3.5 *Potentiodynamic polarization study*

The beneficial effect of Ru towards electro-oxidation of ethanol is further exemplified by a comparison of the

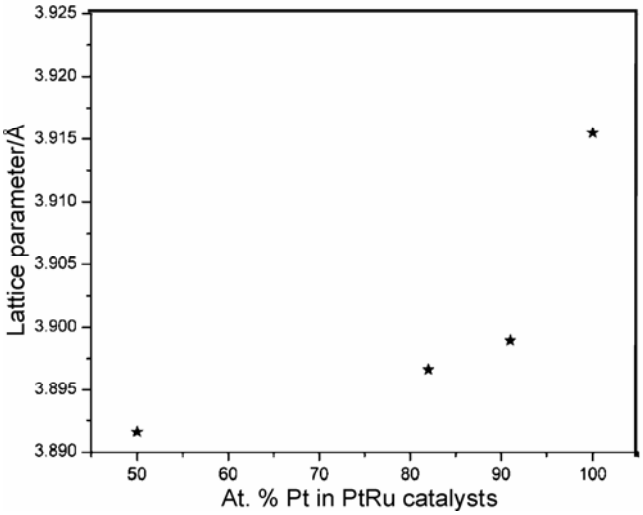

Figure 7. Lattice parameter as function of at.% Pt (as obtained from EDX) in PtRu catalysts.

polarization current densities. Figure 10 shows the current-potential behaviour during potentiodynamic polarization studies at a scan rate of 1 mV s^{-1} of ethanol electro-oxidation on Pt and PtRu electrodes of different compositions. At a potential of –0·2 V, there is a ten-fold increase in current density of $Pt_{82}Ru_{18}$ compared to Pt. More significantly a negative shift of about 150 mV is observed at $Pt_{82}Ru_{18}$ compared to Pt. The $Pt_{82}Ru_{18}$ alloy electrode shows the best polarization behaviour over the entire potential range studied. The higher electrocatalytic activity for the binary PtRu deposits is easily explained on the basis of the promoting effect of Ru for the electro-oxidation of alcohols in acid medium.

3.6 *Chronoamperometric studies*

In order to ascertain the long-term stability of the electrodes, chronoamperograms were also recorded at –0·1 V for 1 h. In all the chronoamperometric curves (figure 11), there is a sharp initial current drop followed by a slower decay. As can be seen, the polarization current recorded for the $Pt_{82}Ru_{18}$ electrode, even for a span of 1 h, produces the highest oxidation current which is almost five

times higher than that obtained with Pt. Taking into account that ensembles of Pt surface atoms are required for the adsorption of ethanol on Pt and that ethanol does not adsorb on Ru, it follows that the promoter atoms should be present in low amounts. It may be said that

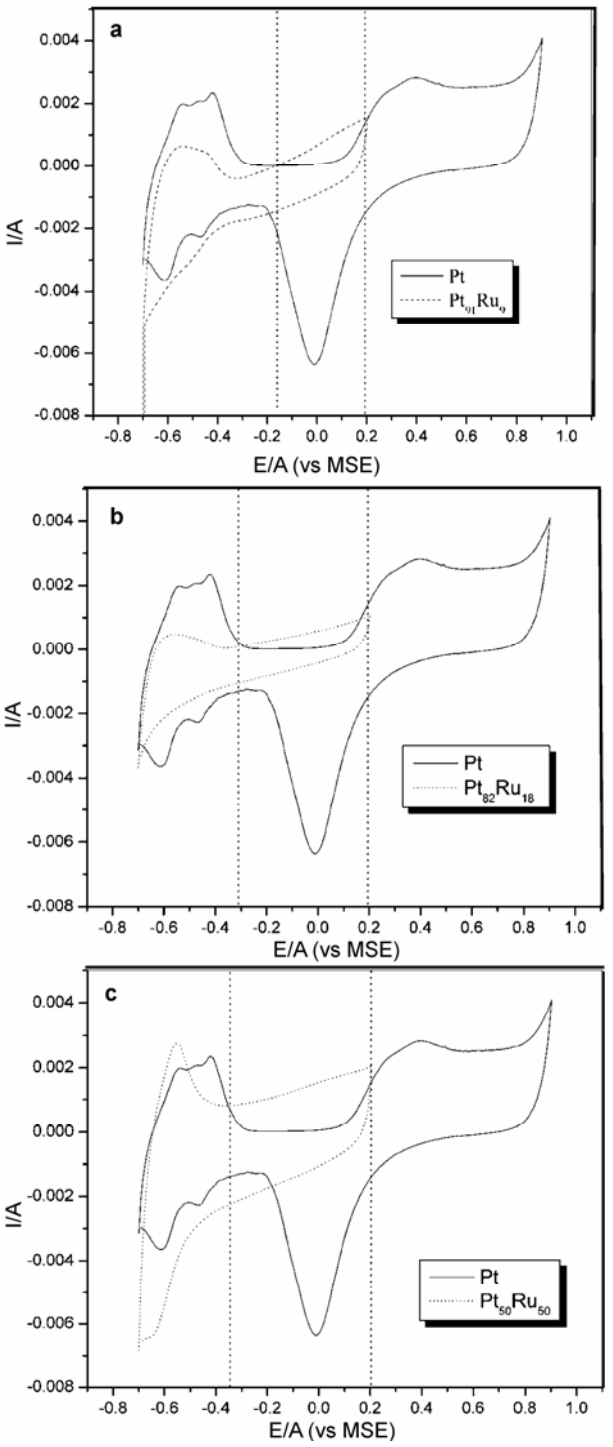

Figure 8. Comparison of cyclic voltammograms in 0·5 M H_2SO_4 of Pt with **a**. $Pt_{91}Ru_9$ (scan rate = 50 mV s^{-1}), **b**. $Pt_{82}Ru_{18}$ (scan rate = 50 mV s^{-1}) and **c**. $Pt_{50}Ru_{50}$ (scan rate = 50 mV s^{-1}).

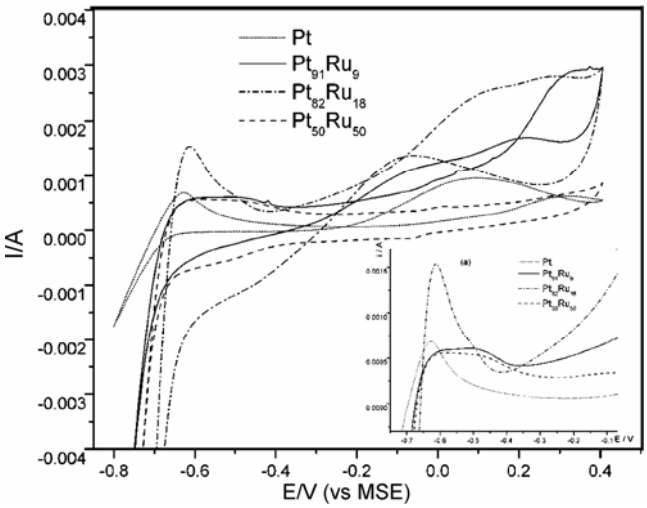

Figure 9. Comparison of cyclic voltammograms in 1 M EtOH of Pt with different compositions of PtRu (scan rate = 50 mV s^{-1}).

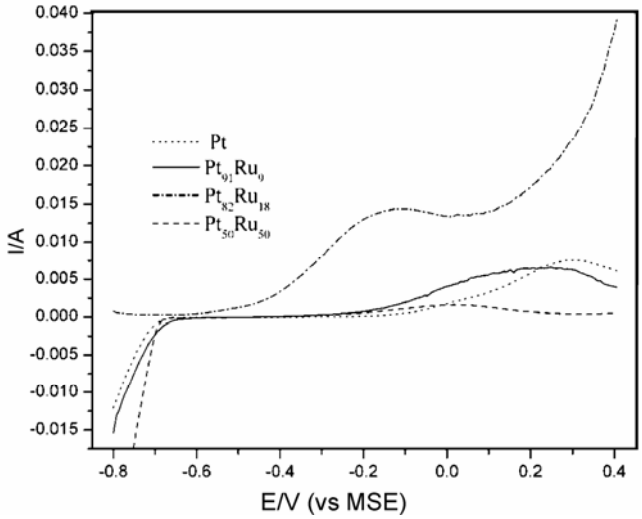

Figure 10. Potentiodynamic polarization plots obtained in 1·0 M ethanol and 0·5 M H_2SO_4 at a scan rate of 1 mV s^{-1}.

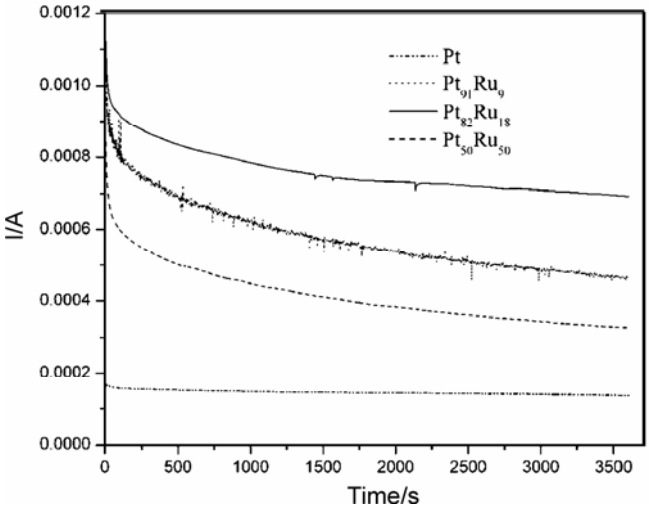

Figure 11. Chronoamperograms recorded at –0·1 V for Pt and PtRu electrocatalysts in 0·5 M H_2SO_4 + 1·0 M EtOH.

Table 3. Values of the electrical elements obtained by fitting the impedance data at – 0·1 V with the equivalent circuits shown in figures 15a and b.

Catalyst	R_s (ohm)	CPE × 10^3	R_{ct} (ohm)	C_P (mF)	R_∞ (ohm)	Frequency of $-\phi_{max}$ (mHz)
Pt	14·62	2·303	8100	–	–	205·4
$Pt_{91}Ru_9$	3·90	2·510	431·3	2·98	416	2376·0
$Pt_{82}Ru_{18}$	1·85	3·420	215·9	7·11	26·33	6790·0
$Pt_{50}Ru_{50}$	9·54	2·295	8030	3·26	120	991·0

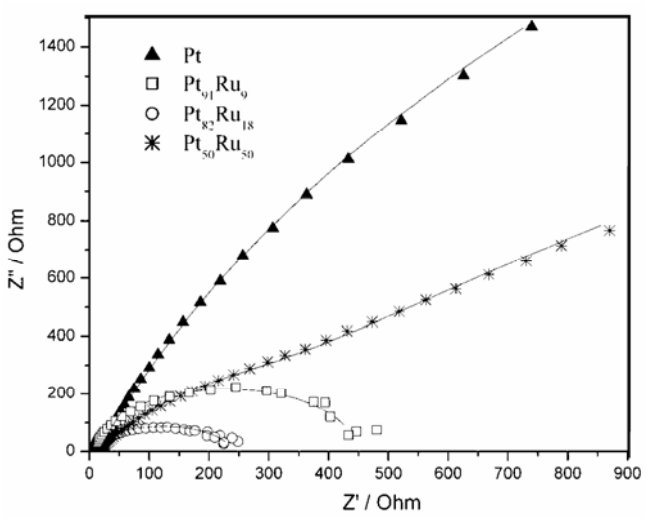

Figure 12. Nyquist plots (equivalent circuit fitted) of ethanol oxidation at a potential of –0·10 V.

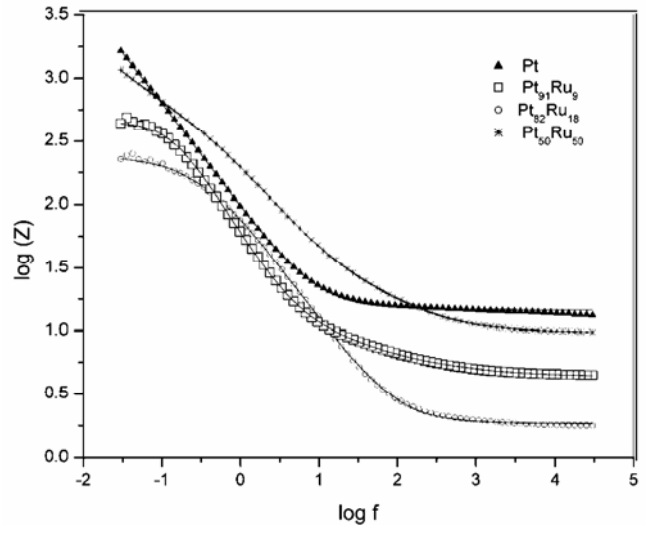

Figure 13. Bode plot–frequency vs total impedance of unsupported Pt and PtRu at different compositions.

sufficient number of Pt sites enabling the reaction to proceed to the CO_{ads} stage is the prerequisite for Ru to act via oxygen transfer. This is tenable with our results for an activity maximum with ~18 at.% Ru catalyst.

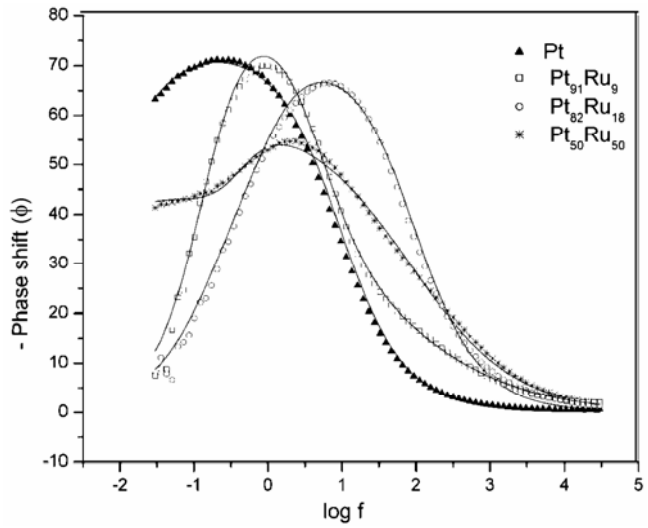

Figure 14. Bode plot-frequency vs phase angle of unsupported Pt and PtRu at different compositions.

3.7 *Electrochemical impedance spectroscopy*

Nyquist plots obtained for ethanol oxidation on the unsupported Pt and PtRu electrodes in 1 M ethanol and 0·5 M H_2SO_4 at –0·1 V vs MSE are presented in figure 12. The complex-plane impedance of unsupported Pt shows almost a line with an initial slope close to 90° along the imaginary axis (Z''), characteristic of an ideally polarizable electrode as in an electric double-layer capacitor. A slight deviation from the straight line is observed at low frequency (<0·1 Hz), which may be an indication of the commencement of the dissociative ethanol adsorption. The complex-plane plots for $Pt_{91}Ru_9$ and $Pt_{82}Ru_{18}$ are evidenced by the formation of arc which indicates the presence of a resistive component. The transition from capacitive behaviour to resistive behaviour is more clearly evident in the corresponding Bode plots (figures 13 and 14). The transformation behaviour can be distinguished by a characteristic frequency where the –Φ value exhibits a maximum i.e. the deviation from the –90° phase angle (Sugimoto *et al* 2005). The phase angle is almost constant down to 10 MHz for unsupported Pt. Therefore, the electrode reaction is dominated by the electric double-layer capacitance and the electrocatalysis is small within the frequency range studied. A maximum appears in the –Φ

value in the Bode plots for Pt below –0·07 Hz and the characteristic frequency increases to higher frequency in the order $Pt < Pt_{91}Ru_9 < Pt_{50}Ru_{50} < Pt_{82}Ru_{18}$ which implies that predominance of the resistive behaviour is translated to increased electroactivity (as shown in table 3). Based on these observations, it may be stated that an optimum Ru content in binary PtRu catalysts for ethanol oxidation is reached at 18% Ru levels. The impedance data of unsupported Pt were fitted using the equivalent circuit shown in figure 15(a), where a parallel constant-phase element (CPE)-resistor (R_{ct}) combination was added in series of solution resistance (Rs). Here, CPE and R_{ct} are the frequency-dependent capacitance and charge-transfer resistance, respectively at the outermost surface of the electrode. A capacitor (C_P) was also used for the electric double-layer capacitance to account for the porous PtRu. The fit based on the modified equivalent circuit (figure 15(b)) agrees well with the experimental data throughout the whole frequency range studied. The value of capacitance was in the range 2–8 mF (as shown in table 3) which is a reasonable value for the electrical double-layer capacitance. The reaction resistance of CH_3CH_2OH to CO_{ad} (R_∞) which was combined in parallel with capacitor (C_P) decreases with increase of Ru content with a minimum value for $Pt_{82}Ru_{18}$ electrode as shown in table 3. The values reflect that there should be an optimum ratio of Pt to Ru sites for both the dissociative adsorption of ethanol as well as the subsequent CO oxidation step at lower overpotential. This is best satisfied by the $Pt_{82}Ru_{18}$ electrode.

4. Conclusions

This work deals with the study of electro-oxidation of ethanol on Pt based alloy catalysts containing different atomic percentages of Ru which were synthesized by borohydride reduction method. Based on the results obtained from different electrochemical techniques like CV, polarization studies, EIS and chronoamperometry employed for the study of electrocatalytic behaviour of different catalysts, the $Pt_{82}Ru_{18}$ alloy was identified as the best composition in promoting ethanol oxidation in acid medium. This is ascribed to the optimum number of Ru sites available in the matrix which is required for the oxidation of adsorbed CO species subsequent to the dissociative adsorption of ethanol at Pt centres. At substantially higher Ru concentration, ethanol adsorption is significantly inhibited as the number of Pt sites available for the purpose is not sufficient. On the other hand, at low Ru concentration, there are possibly not enough Ru sites to effectively oxidize the adsorbed CO and catalytic activity remains low.

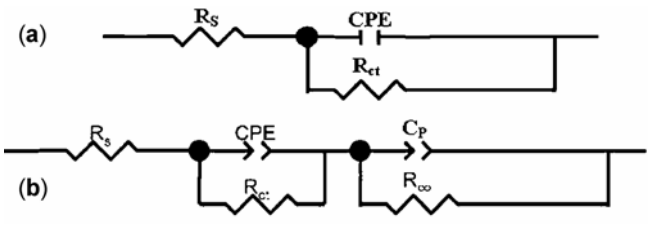

Figure 15. (**a**) Equivalent circuit for modeling the impedance data of Pt and (**b**) equivalent circuit for modeling the impedance data of PtRu catalysts.

Acknowledgement

We gratefully acknowledge the Defence Research and Development Organization (DRDO), New Delhi, for financial support.

References

Arico A S, Creti P, Kim H, Mantegna R, Giordano N and Antonucci V 1996 *J. Electrochem. Soc.* **143** 3950

Chen G L, Sun S G, Chen S P and Zhou Z Y 2001 *Chinese Appl. Chem.* **18** 432

Chu D and Gilman S 1996 *J. Electrochem. Soc.* **143** 1686

Colmati F, Lizacano-Valbuena W H, Camara G A, Ticianelli E A and Gonzalez E R 2002 *J. Braz. Chem. Soc.* **13** 474

Colmati F, Antolini E and Gonzalez E R 2007 *J. Electrochem. Soc.* **154** B39

Delime F, Léger J -M and Lamy C 1999 *J. Appl. Electrochem.* **29** 1249

De Souza J P I, Queiroz S L, Bergmaski K, Gonzalez E R and Nart F C 2002 *J. Phys. Chem.* **B106** 9825

Frelink T, Visscher W and Van Veen J A R 1995 *Surface Sci.* **335** 353

Fujiwara N, Tsiakaras P and Stimming U 1999 *J. Electroanal. Chem.* **472** 120

Hogarth M P and Ralph T R 2002 *Platinum Metals Review* **46** 146

Iwasita T 2002 *Electrochim. Acta* **47** 3663

Iwasita T and Pastor E 1994 *Electrochim. Acta* **39** 531, 547

Janssen M M P and Moolhuysen J 1977 *J. Catal.* **46** 289

Laborade H, Rezzouk A, Legér J -M, Lamy C, Srinivasan S, MacDonald D D and Khandkar A C (eds) 1994 *J. Electrochem. Soc.* **94** 275

Lamy C, Belgsir E M and Leger J M 2001 *J. Appl. Electrochem.* **31** 799

Lamy C, Lima A, Le Rhum V, Delime F, Contanceau C and Leger J-M 2002 *J. Power Sources* **105** 283

Li H, Sun G, Cao L, Jiang L and Xin Q 2007 *Electrochim. Acta* **52** 6622

Liu Z, Ling X Y, Su X, Lee J Y and Gan L M 2005 *J. Power Sources* **149** 1

Mahmood T, Williams J O, Miles R and McNicol B D 1981 *J. Catal.* **72** 218

McNicol B D and Short R T 1978 *J. Electroanal. Chem.* **92** 115

O'Hayre R P, Cha S -W, Colella W and Prinz F B 2006 *Fuel cell fundamentals* (New York: John Wiley & Sons, Inc)

Oliveria Neto A, Giz M J, Perez J, Ticianelli E A and Gonzalez E R 2002 *J. Electrochem. Soc.* **149** A272

Pacheo V, Stantos D and Tremiliosi-Filho G *Platinum/osmium as a catalyst for ethanol oxidation* (http://www.Arofe.army.mil/conference/recent abstrac/200th meeting/symposia/h1/1051.pdf)
Rightmire R A, Rowlad R L, Boos D L and Beals D L 1964 *J. Electrochem. Soc.* **111** 242
Spinace E V, Neto A O, Vasconcelos T R R and Linardi M 2004 *J. Power Sources* **137** 17
Song S Q *et al* 2005 *Int. J. Hydrogen Energy* **30** 995
Sugimoto W, Aoyama K, Kawaguchi T, Murakami Y and Takasu Y 2005 *J. Electroanal. Chem.* **576** 215
Vigier F, Coutanceau C, Perrard A, Belgsir E M and Lamy C 2004 *J. Appl. Electrochem.* **34** 439
Volkmar M S, Remo I, Elena P and Sergio G 1996 *J. Phys. Chem.* **100** 17901
Watanabe M and Motoo S 1975a *Electroanal. Chem. & Interf. Electrochem.* **60** 267
Watanabe M and Motoo S 1975b *J. Electroanal. Chem.* **60** 275
Wasmus S and Kuver A 1999 *J. Electroanal. Chem.* **461** 14
Yang C *et al* 2001 *Electrochem. Solid State Lett.* **4** A31
Zhou W J *et al* 2004 *J. Power Sources* **131** 217